Jurnal Sainstech Nusantara	Vol. 2 No. 4 (2025) 25-37
https://nusantarajournal.id/sainstech	ISSN: 3063-0657

Experimental Flow Visualization of a NACA 4412 Airfoil Equipped with a 60° Forward Wingtip Fence in a Subsonic Wind Tunnel

Firja Zahran Rasendriya[1], Suyatmo[1]

[1]Aircraft Engineering Study Program, Surabaya Aviation Polytechnic, Jl. Jemur Andayani I/73 Wonocolo Surabaya, East Java, 60236, INDONESIA

Article Info

Article history:

Received 06 July, 2025
Revised 12 October, 2025
Accepted 12 November, 2025

Abstract

Wingtip-induced three-dimensional flow accelerates boundary-layer separation and amplifies vortex-related losses, particularly at low Reynolds numbers. This study experimentally investigates the surface-flow characteristics of a NACA 4412 airfoil equipped with a 60° forward wingtip fence under subsonic conditions. Wind-tunnel experiments were conducted at a freestream velocity of 10 m/s ($Re \approx 2.3 \times 10^4$) over angles of attack ranging from 0° to 17°. Oil-flow visualization and tuft visualization were employed to identify laminar–turbulent transition (Xt), separation (Xs), and reattachment (Xr) locations and to qualitatively assess near-surface flow stability. Compared with the baseline airfoil, the 60° forward wingtip fence systematically shifted separation downstream and delayed vortex development in the pre-stall regime. At 10°, the separation point moved from approximately 20 mm (baseline) to 30 mm, while reattachment shifted from 30 mm to 45 mm. Tuft observations indicate that significant vortex formation appeared earlier in the plain configuration (from 12°), whereas the fenced configuration maintained comparatively stable flow up to 12° and exhibited pronounced instability primarily at 15°–17°. The results demonstrate that a 60° forward wingtip fence enhances upper-surface flow stability and postpones separation onset at low Reynolds numbers, providing experimental guidance for compact wingtip-device optimization.

Keyword: Wingtip fence , NACA 4412, wingspan, angle of attack, wind tunnel

Corresponding Author:

Suyatmo
Email: suyatmo.marto1963@poltekbangsby.ac.id

1. Introduction

In aerodynamic design, the wingtip represents a critical region where three-dimensional flow structures strongly influence the overall performance of a lifting surface. The pressure difference between the lower (pressure) and upper (suction) surfaces drives spanwise flow near the tip, leading to vortex formation and increased induced drag. This phenomenon not only reduces lift-to-drag

DOI: https://doi.org/10.71225/jstn.v2i4.120

efficiency but also accelerates boundary-layer separation at elevated angles of attack. Consequently, wingtip-device concepts have received sustained attention because relatively minor geometric modifications at the tip can produce measurable improvements in aerodynamic performance [1]. In both aviation education and applied research contexts, the development of practical, manufacturable, and aerodynamically effective wingtip configurations remains an important engineering challenge [2], [3].

To mitigate wingtip-induced losses, various add-on devices have been proposed, including vortex generators, winglets, wingtip fences, flaps, slats, and slots. These devices are generally intended to regulate boundary-layer development, weaken tip-vortex intensity, and delay separation, thereby improving lift characteristics and/or reducing drag penalties. Among these approaches, wingtip fences are particularly attractive due to their structural simplicity, ease of integration, and suitability for small-scale platforms [4] [5] [6] [7]. However, their aerodynamic effectiveness depends strongly on geometric parameters such as cant angle and orientation, and the associated flow mechanisms must be validated experimentally, especially under low-to-moderate Reynolds number conditions where boundary-layer sensitivity is pronounced [9] [10] [11] [12].

Previous studies have provided preliminary evidence that wingtip fence orientation significantly influences near-tip flow behavior. Juniarwanto (2021) examined forward and rearward wingtip fence configurations with a 75° cant angle on an Eppler E562 airfoil using oil-flow visualization, reporting modifications in separation patterns and inferred pressure distribution [8], [9]. Similarly, Hariyadi (2020) employed tuft visualization for a 75° forward wingtip fence on the same airfoil and observed reduced turbulence signatures at moderate angles of attack, although unsteadiness intensified at higher angles. While these studies indicate that forward-oriented wingtip fences can influence separation tendencies, the available experimental evidence remains largely restricted to a single cant angle (75°) and a specific airfoil family, leaving limited understanding of how alternative cant angles perform on different airfoil geometries [8] [9] [13] [14] [15].

Despite these contributions, there remains insufficient experimental clarity regarding how a forward wingtip fence with a lower cant angle modifies transition, separation, and reattachment behavior on a widely used cambered airfoil such as the NACA 4412. This airfoil is relevant to subsonic applications and exhibits boundary-layer characteristics that may respond differently to wingtip modifications compared with Eppler-series profiles. Therefore, the present study aims to experimentally evaluate the surface-flow response of a NACA 4412 airfoil equipped with a 60° forward wingtip fence under subsonic wind-tunnel conditions. Oil-flow and tuft visualization techniques are employed to examine near-surface streamline patterns, identify transition and separation-related features, and compare the modified configuration against the baseline across a range of angles of attack. By systematically analyzing the influence of a 60° cant angle at low Reynolds number, this work contributes experimentally grounded insight into the aerodynamic optimization of compact wingtip-fence configurations.

2. Research Method

This experiment uses the NACA 4412 airfoil type with a modification that adds a front wingtip. Fence cant angle of 60º to assess the airfoil's performance with Forward Wingtip added Fence cannot be angled 60 degrees and is equivalent to an airfoil without wingtip.

Table 1. Parameter Eksperimen Wingtip Fence

Parameter	Eksperimen
Shape	Wingtip Fence 60º

DOI: https://doi.org/10.71225/jstn.v2i4.120

Airfoil Chord, c	72mm
Upper winglet height, h1	72mm
Lower winglet height, h2	72mm
Wingtip minimum chord, w	15.20mm
Wingtip maximum chord, w	72mm
Type wingtip	Forward Wingtip Fence
AoA	0º, 4º, 10º, 12º, 15º, 17º
Speed/ v	10m/s
Length / l	300mm

Figure 1. depicts the geometry and installation orientation of the forward wingtip fence mounted at the wingtip of the airfoil model (spanwise length 300 mm). The fence is arranged with a cant angle of 60° relative to the local wing reference plane, with an additional 30° reference angle indicated to define the installation orientation at the tip. The planform of the fence is specified by an upper and lower height of 72 mm each, a minimum tip chord of 15.20 mm, and a characteristic base width of 72 mm, while the main outline incorporates two 35° edge angles and an internal angle of 75° as shown. A three-dimensional rendering is provided to illustrate the final assembled configuration, confirming that the fence forms a canted, forward-oriented surface at the wingtip consistent with the forward wingtip fence concept used in the experiments [16] [17].

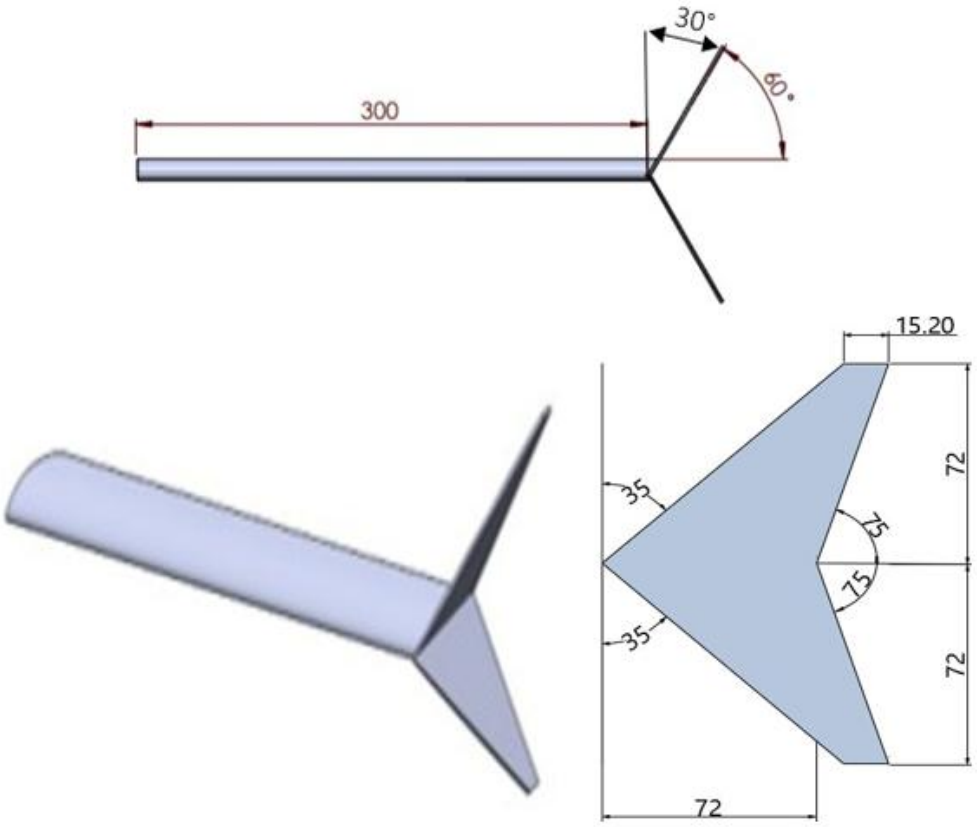

Figure 1. Airfoil object model

Wind-tunnel experiments were conducted using an open-circuit subsonic wind tunnel. The facility was powered by a 240 V/50 Hz electrical supply with an installed capacity of 1.5 kW and had overall dimensions of 2980 mm × 1830 mm × 800 mm. The test/working section comprised an

DOI: https://doi.org/10.71225/jstn.v2i4.120

octagonal working section with an equivalent dimension of 300 mm and a length of 450 mm, while the main test section employed a rectangular cross-section with a length of 1800 mm, a height of 660 mm, and a width of 660 mm. The tunnel provided a maximum freestream velocity of 50 m/s. Aerodynamic forces were monitored using an integrated balance system with a maximum lift capacity of 7.0 N and a maximum drag capacity of 2.5 N, with a stated measurement sensitivity of 0.01 N. A schematic of the open-circuit wind tunnel used in this study is shown in Figure 2

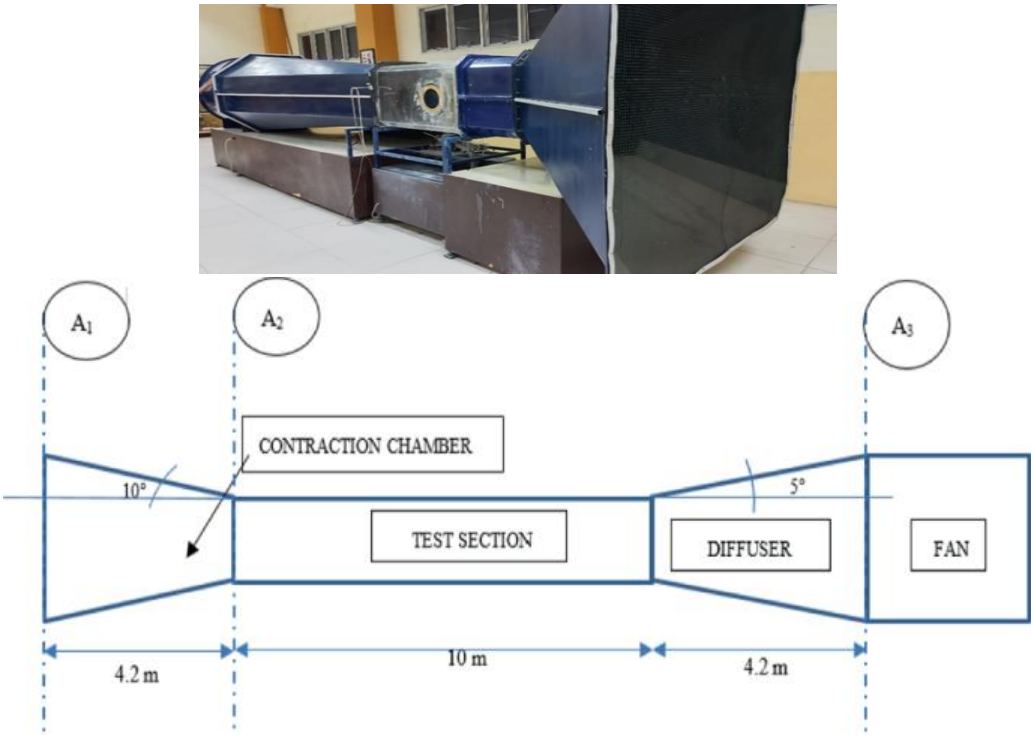

Figure 2. Open circuit wind tunnel

Oil-flow visualization was employed to examine near-wall flow structure on the upper surface of the airfoil by tracking the redistribution of a thin oil–pigment film under aerodynamic shear. Before each test, the surface was coated with a uniformly thin layer of an oil mixture; during tunnel operation, the film was driven by local wall shear stress, forming streaklines and accumulation zones that qualitatively represent surface streamlines and indicate changes in boundary-layer behavior, including regions associated with separation and reattachment. After an adequate exposure time, the film partially dried and the resulting patterns were recorded for analysis. The oil mixture was prepared by first combining kerosene and titanium dioxide (TiO_2) powder at a volumetric ratio of 5:1 and mixing for 15 min to obtain a homogeneous suspension, followed by the addition of oleic acid as a viscosity/binding agent at a volumetric ratio of 1:20 to regulate film mobility and produce clear, high-contrast traces [7] [8].

Tuft visualization was additionally used as a complementary qualitative technique to interpret airflow patterns along the airfoil surface, particularly to identify unsteady flow, local flow reversal, and vortex-related disturbances. In this method, small tufts made of fine thread were attached to the airfoil surface in a predetermined grid to indicate instantaneous local flow direction. For the present investigation, the tuft grid spacing was set to 1 cm, with a thread length of 3 inches. The NACA 4412 airfoil was tested in the wind tunnel across multiple angles of attack, both in the baseline configuration and with the addition of a 60° forward wingtip fence, and the recorded tuft behavior was used to assess the evolution of surface-flow stability as the angle of attack increased [5] [6] [7].

DOI: https://doi.org/10.71225/jstn.v2i4.120

3. Results And Discussion

3.1 Transition, Separation, and Reattachment Analysis

The analysis of transition (X_t), separation (X_s), and reattachment (X_r) points was conducted to evaluate the influence of the 60° forward wingtip fence on the upper-surface boundary-layer development of the NACA 4412 airfoil at $Re = 2.3 \times 10^4$. The extracted streamwise locations for both the plain airfoil and the modified configuration are illustrated in Figure 3.

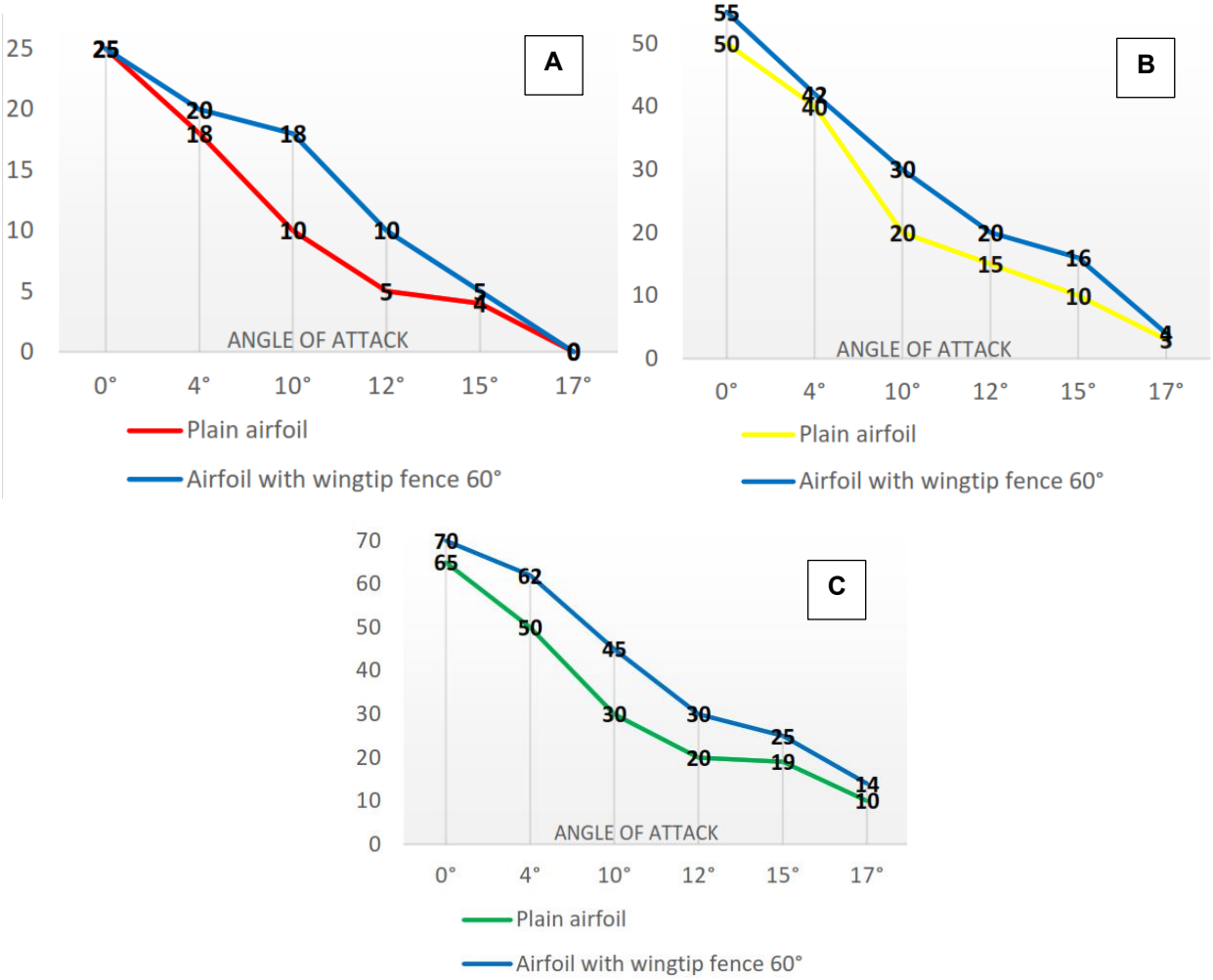

Figure 3. (a) Transition point (b) Sparation point (c) Reattachment point

For the plain airfoil, the transition point progressively shifts upstream as the angle of attack increases, indicating earlier laminar–turbulent transition under stronger adverse pressure gradients. At 0°, the transition occurs at 25 mm from the leading edge, moving to 18 mm at 4°, 10 mm at 10°, 5 mm at 12°, and 4 mm at 15°. This upstream migration reflects increased instability in the boundary layer as the effective suction peak near the leading edge intensifies. A similar trend is observed for separation and reattachment points: at 0°, separation occurs at 50 mm and reattachment at 65 mm, while at 10° separation moves upstream to 20 mm with reattachment at 30 mm. At higher angles (12°–15°), separation occurs very close to the leading edge, indicating the onset of significant flow detachment and approach toward stall conditions [16] [17].

DOI: https://doi.org/10.71225/jstn.v2i4.120

In contrast, the airfoil equipped with the 60° forward wingtip fence demonstrates a consistent downstream shift of the separation and reattachment points at low-to-moderate angles of attack. At 0°, separation occurs at 55 mm and reattachment at 70 mm, compared with 50 mm and 65 mm for the plain airfoil. At 10°, separation shifts from 20 mm (plain) to 30 mm (with fence), and reattachment from 30 mm to 45 mm. This downstream displacement indicates that the forward wingtip fence delays separation and extends the region of attached flow along the upper surface. The transition point also follows a comparable upstream trend with increasing angle of attack; however, its movement is slightly moderated in the fenced configuration at moderate angles, suggesting improved flow stability. At 12° and 15°, although both configurations experience significant upstream movement of separation due to intensified adverse pressure gradients, the fenced configuration still maintains slightly more favorable separation and reattachment locations (e.g., at 15°: $X_s = 16$mm with fence vs. 10 mm for plain airfoil). At 17°, separation in the fenced configuration occurs at 4 mm with reattachment at 14 mm, indicating dominant leading-edge separation and strongly turbulent flow, consistent with near-stall behavior [18] [19].

The comparative trends presented in Figure 6 clearly demonstrate that the inclusion of a 60° forward wingtip fence improves boundary-layer attachment characteristics in the pre-stall regime. Because earlier separation (i.e., closer to the leading edge) is associated with stronger turbulence development and reduced aerodynamic efficiency, the observed downstream shift of $X_s$in the modified configuration confirms that the wingtip fence effectively suppresses premature separation. This behavior can be attributed to the fence-induced modification of three-dimensional tip flow, which reduces spanwise pressure-driven leakage and weakens vortex interaction with the upper surface. Consequently, the 60° forward wingtip fence enhances flow stability and delays the onset of large-scale separation compared with the plain airfoil, particularly at low-to-moderate angles of attack [20].

3.2 Oil-Flow Visualization

Oil-flow visualization was employed to identify boundary-layer behavior, including transition, separation, and reattachment phenomena, on the upper surface of the NACA 4412 airfoil with and without the 60° forward wingtip fence. This method enables clear detection of laminar-to-turbulent transition and separated-flow regions through characteristic streakline patterns formed after the oil mixture dries under wind-tunnel operation (Re = 2.3 × 10⁴; $U_\infty = 10$m/s). At low angles of attack (0° and 4°), both configurations exhibit relatively smooth and aligned oil streaklines, indicating predominantly attached flow with no significant separation. However, as the angle of attack increases to 10°, distinct differences between the two configurations become evident. For the plain airfoil, separation occurs at approximately 20 mm from the leading edge, followed by reattachment at 30 mm, as identified from the disruption and subsequent realignment of oil streaklines. In contrast, the airfoil equipped with the 60° forward wingtip fence exhibits delayed separation at approximately 30 mm and reattachment at 45 mm. This downstream shift of both separation and reattachment points demonstrates that the forward wingtip fence modifies the upper-surface flow structure and extends the region of attached boundary-layer flow at moderate angles of attack. At 12°, the plain airfoil shows earlier boundary-layer transition and a more extensive separated region compared with the modified configuration [21] [22]. The oil patterns become increasingly irregular near the mid-chord, indicating strengthened adverse pressure gradients and accelerated instability growth. Meanwhile, the airfoil with the forward wingtip fence still maintains comparatively more organized streaklines, suggesting improved flow attachment and delayed separation development. At higher angles of attack (15° and 17°), both configurations exhibit pronounced turbulent activity near the leading edge. The oil-flow patterns reveal significant disruption and chaotic streakline structures, indicating strong

DOI: https://doi.org/10.71225/jstn.v2i4.120

separation and large-scale vortex formation. In these conditions, the boundary layer transitions rapidly from laminar to turbulent due to the intensified adverse pressure gradient at the leading edge. Although the forward wingtip fence continues to slightly modify the separation topology, its ability to delay separation becomes limited as the airfoil approaches stall-like conditions. Overall, the oil-flow visualization results confirm that the addition of a 60° forward wingtip fence effectively delays separation and shifts the reattachment point downstream in the low-to-moderate angle-of-attack regime. This indicates improved upper-surface flow stability and reduced premature separation compared with the plain airfoil. However, at higher angles of attack (15°–17°), both configurations experience dominant turbulent separation, suggesting that the aerodynamic benefit of the forward wingtip fence is most significant prior to stall onset [23] [24].

Figure 4. Tuft visualization (a) 0º (b) 4º (c) 10º (d) 12º (e) 15º (f) 17º

The processed fluid-flow visualizations presented in Figures 4 (angle of attack 0°–17°) provide additional insight into the evolution of upper-surface flow structures as the angle of attack

DOI: https://doi.org/10.71225/jstn.v2i4.120

increases and clarify the aerodynamic role of the 60° forward wingtip fence. As observed in the 0° images (Figure 12), both the plain airfoil and the modified configuration exhibit relatively uniform color gradients and smooth contour distributions, indicating attached flow and stable boundary-layer development. However, as the angle of attack increases progressively to 4° and 10° (Figures 13 and 14), subtle differences begin to emerge: the plain airfoil shows earlier distortion of contour lines near the mid-chord and trailing-edge regions, whereas the airfoil with the forward wingtip fence maintains a more coherent and aligned flow pattern [25].

At higher angles of attack (12°, 15°, and 17°; Figures 15–17), the contrast becomes more pronounced. The plain airfoil exhibits increasingly irregular contour distributions and concentrated high-gradient regions near the leading edge and mid-chord, indicating stronger adverse pressure gradients and earlier transition from laminar to turbulent boundary-layer flow. The rise in pressure at the leading edge with increasing angle of attack accelerates flow instability, promoting premature boundary-layer transition and separation. This behavior is particularly evident at 17°, where the contour pattern on the plain airfoil appears highly distorted, consistent with extensive separation and vortex-dominated flow. In contrast, the airfoil equipped with the 60° forward wingtip fence shows comparatively smoother contour transitions and more organized flow structures up to moderate angles of attack. Although instability becomes evident at 15° and 17°, the spatial extent and intensity of contour distortion remain comparatively reduced, suggesting delayed separation and moderated vortex growth [26].

The novelty of this study lies in the integrated experimental comparison between oil-flow visualization, tuft visualization, and image-based contour processing for a NACA 4412 airfoil equipped with a 60° forward wingtip fence at low Reynolds number ($Re = 2.3 \times 10^4$). Unlike previous studies that primarily focused on different cant angles (e.g., 75° configurations) or alternative airfoil geometries, this investigation demonstrates that a 60° forward wingtip fence effectively modifies three-dimensional tip flow interactions in a moderate-Reynolds-number regime typical of small-scale aerodynamic applications. The combined visualization approach reveals that the forward wingtip fence not only shifts the separation point downstream but also alters the spatial development of pressure-induced instability along the leading edge, thereby delaying the laminar–turbulent transition and large-scale vortex formation. This integrated qualitative evidence strengthens the understanding of how specific cant-angle geometry influences upper-surface flow stability, providing experimentally grounded insight into wingtip-fence optimization for low-speed aerodynamic systems [27] [28].

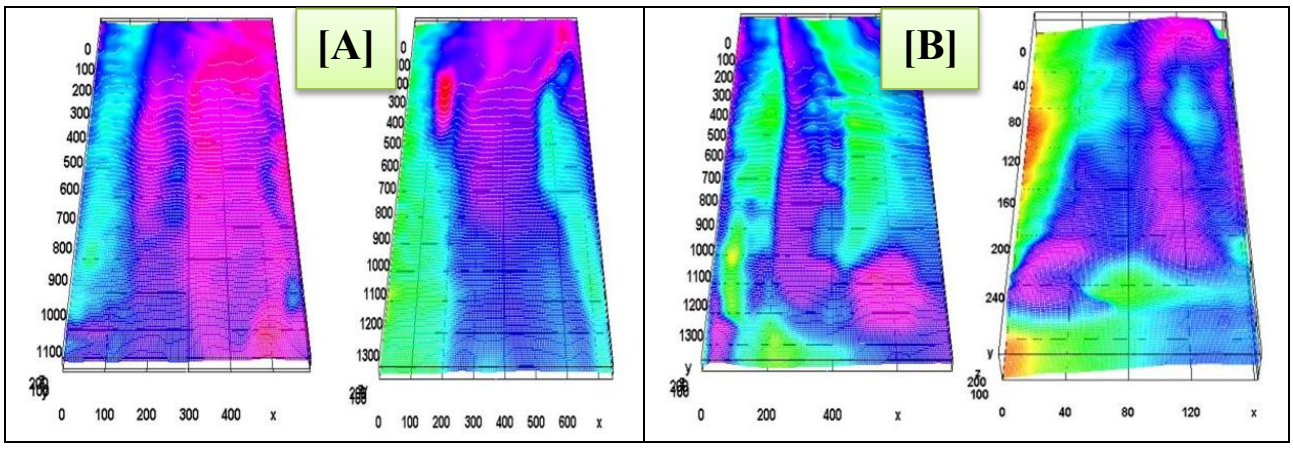

DOI: https://doi.org/10.71225/jstn.v2i4.120

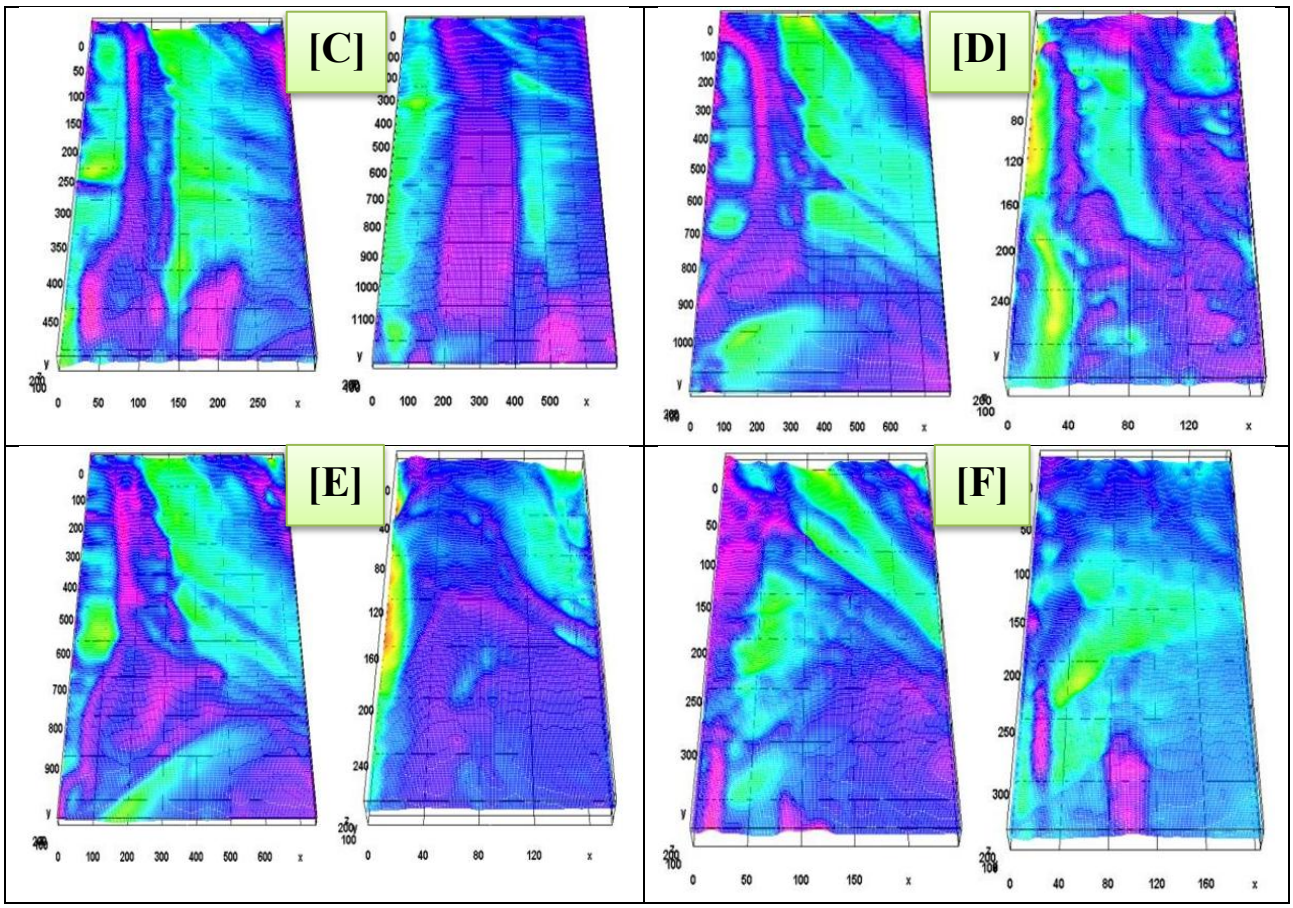

Figure 5. Tuft visualization (a) 0º (b) 4º (c) 10º (d) 12º (e) 15º (f) 17º

3.3 Result tuft visualization

Tuft visualization was employed to qualitatively examine the development of surface flow structures on the upper surface of the NACA 4412 airfoil, both in the plain configuration and with the addition of a 60° forward wingtip fence. This technique enables direct observation of near-surface flow directionality, unsteadiness, and the onset of vortex formation, thereby providing insight into boundary-layer behavior and separation characteristics across the tested angles of attack (0°, 4°, 10°, 12°, 15°, and 17°).

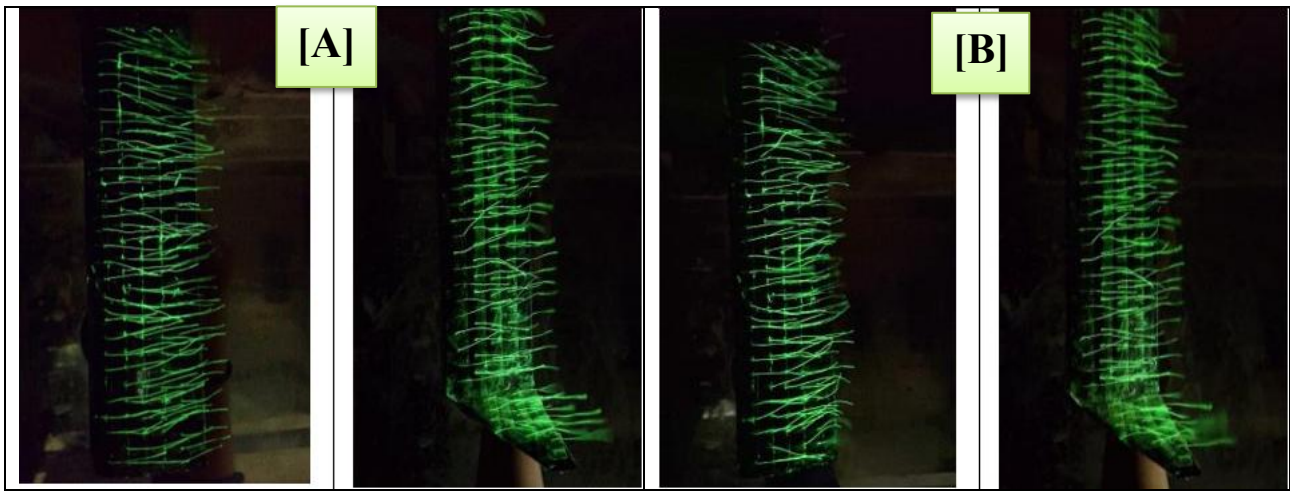

DOI: https://doi.org/10.71225/jstn.v2i4.120

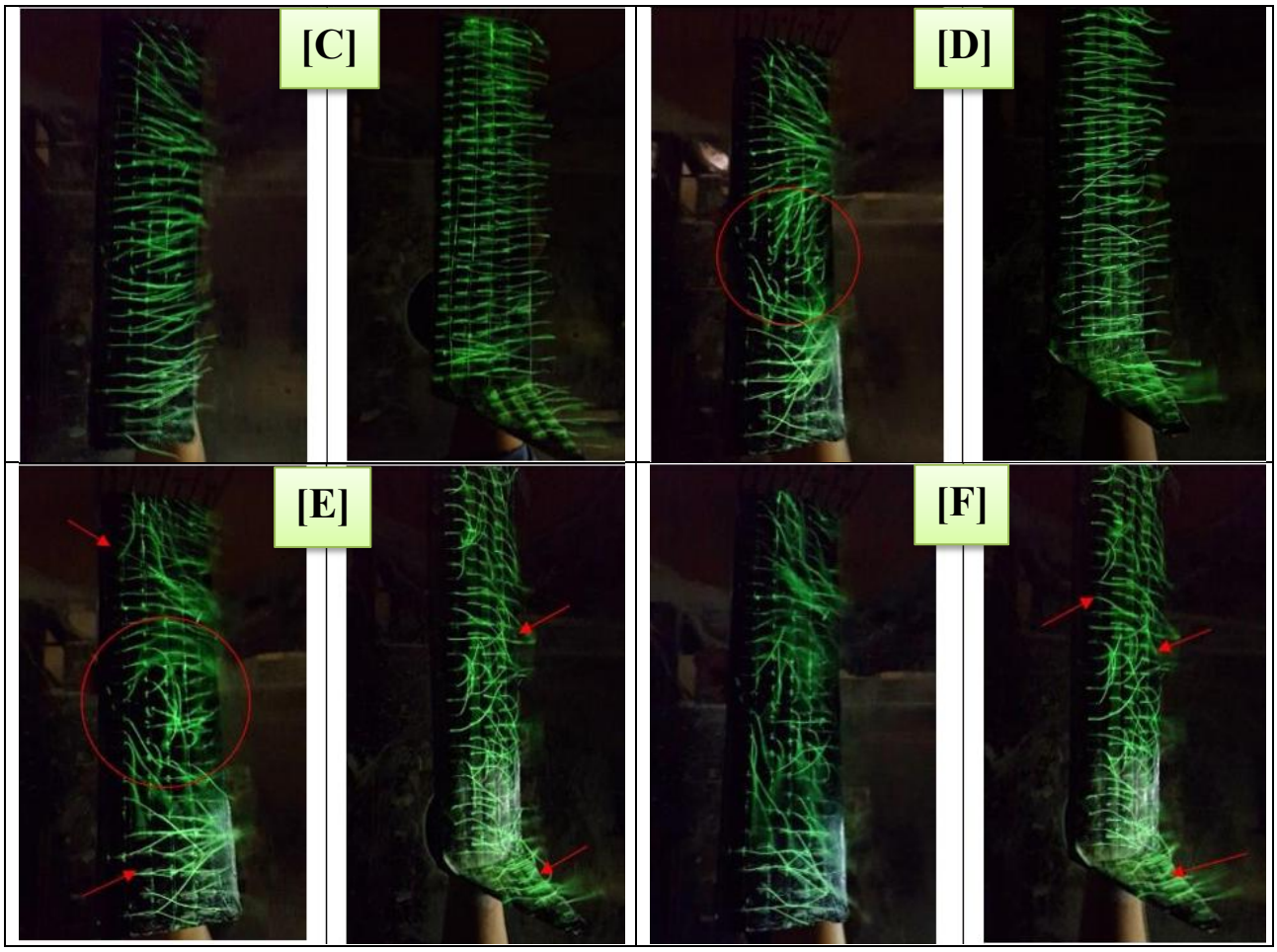

Figure 6. Tuft visualization

For the plain airfoil configuration, the tuft patterns at 0° and 4° angles of attack exhibit stable and uniformly aligned fibers, indicating fully attached flow with no visible vortex formation. At 10°, a small vortex structure becomes apparent near the trailing-edge region, suggesting the initial development of localized flow separation. As the angle of attack increases to 12°, vortex formation becomes clearly visible in the central region of the airfoil, reflecting the strengthening adverse pressure gradient and the early onset of large-scale flow instability. At 15°, a pronounced vortex is observed in the mid-chord region, accompanied by increasingly irregular tuft orientation extending from the leading edge to the trailing edge. At 17°, the vortex structures become more extensive along the spanwise direction, and the tuft motion appears highly irregular, indicating significant flow separation and enhanced turbulence intensity. These observations confirm that, in the plain airfoil configuration, large-scale unsteady flow and separation phenomena develop relatively early, becoming evident from approximately 12° and intensifying at higher angles of attack [5] [6] [7].

In contrast, the airfoil equipped with the 60° forward wingtip fence demonstrates improved flow stability over a broader angle-of-attack range. At 0° and 4°, the tuft alignment remains stable and uniform, similar to the plain configuration, with no evidence of vortex formation. At 10°, the flow remains largely attached and stable, with no significant vortex structures detected, indicating that the addition of the wingtip fence does not introduce premature disturbances at moderate angles of attack. At 12°, only a slight vortex is observed near the wingtip region, while the central and trailing-edge areas remain comparatively stable. More pronounced vortex development becomes evident at

DOI: https://doi.org/10.71225/jstn.v2i4.120

15°, primarily concentrated near the wingtip, and begins to extend toward the trailing edge. At 17°, larger vortex structures are visible along the airfoil, and the tuft patterns become irregular, signifying the progression toward substantial separation.

Comparative analysis between the two configurations reveals that the onset of significant vortex formation is delayed in the airfoil equipped with the 60° forward wingtip fence. While the plain airfoil exhibits clear central vortex structures from 12°, the modified configuration maintains relatively stable flow until approximately 15°. This delay in vortex growth indicates that the forward wingtip fence effectively modifies the three-dimensional tip flow, likely by suppressing spanwise crossflow and weakening tip-vortex interaction with the upper surface. Consequently, the boundary layer remains attached over a larger portion of the chord at moderate angles of attack. Although tuft visualization does not directly quantify aerodynamic forces, the observed delay in vortex development suggests improved flow attachment and reduced premature separation in the pre-stall regime. Since early vortex formation and large-scale separation are typically associated with lift degradation and drag increase, the delayed onset observed in the 60° forward wingtip fence configuration implies enhanced aerodynamic stability at moderate angles of attack. However, at higher angles (15°–17°), both configurations exhibit substantial vortex growth and irregular flow behavior, indicating that the beneficial influence of the fence diminishes as stall conditions are approached. Overall, the tuft visualization results provide consistent qualitative evidence that the 60° forward wingtip fence enhances upper-surface flow stability and postpones the development of large-scale vortical structures compared with the plain airfoil configuration within the investigated operating range [20] [21] [27].

4. Conclusion

The present experimental investigation demonstrates that the implementation of a 60° forward wingtip fence on the NACA 4412 airfoil significantly improves upper-surface flow behavior compared with the plain configuration within the tested Reynolds number ($Re = 2.3 \times 10^4$) and angle-of-attack range (0°–17°). Flow-visualization results consistently indicate that the 60° wingtip fence delays the onset of separation by shifting the separation point downstream (e.g., at 0°: 50 mm to 55 mm; at 10°: 20 mm to 30 mm) and correspondingly modifies the reattachment location, thereby promoting a more stable boundary-layer development in the low-to-moderate angle-of-attack regime. Tuft observations further confirm that vortex formation occurs earlier in the plain airfoil (clearly evident from 12° and intensifying at 15°–17°), whereas the forward wingtip fence postpones significant vortex growth until higher angles of attack (15°–17°). These findings indicate that the 60° forward wingtip fence enhances flow stability and mitigates premature separation, which is commonly associated with lift degradation and drag increase. Nevertheless, at higher angles of attack approaching stall conditions, both configurations exhibit strong unsteadiness and vortex development, suggesting that the beneficial effect of the fence is most pronounced in the pre-stall regime. Overall, within the limitations of visualization-based measurements, the 60° forward wingtip fence can be concluded to provide improved aerodynamic flow characteristics relative to the plain airfoil configuration.

Acknowledgements

The authors gratefully acknowledge the Surabaya Aviation Polytechnic for providing wind-tunnel facilities and technical support throughout the experimental campaign. Appreciation is also extended to the Aircraft Engineering Study Program laboratory staff for their assistance in model fabrication, instrumentation setup, and data acquisition. The constructive academic environment and institutional support were instrumental in the successful completion of this research

DOI: https://doi.org/10.71225/jstn.v2i4.120

References

[1] E. Turanoguz and N. Alemdaroglu, “Design of a medium range tactical UAV and improvement of its performance by using winglets,” 2015 International Conference on Unmanned Aircraft Systems, ICUAS 2015, no. June 2015, pp. 1074–1083, 2015.

[2] S. G. Kontogiannis, D. E. Mazarakos, and V. Kostopoulos, “ATLAS IV wing aerodynamic design: From conceptual approach to detailed optimization,” Aerospace Science and Technology, vol. 56, pp. 135–147, 2016.

[3] N. Mulvany, L. Chen, J. Tu, and B. Anderson, “Steady-State Evaluation of Two-Equation RANS (Reynolds-Averaged Navier-Stokes) Turbulence Models for High-Reynolds Number Hydrodynamic Flow Simulations,” Department of Defense, Australian Government, pp. 1–54, 2004.

[4] E. Turanoguz and N. Alemdaroglu, “Design of a medium range tactical UAV and improvement of its performance by using winglets,” 2015 International Conference on Unmanned Aircraft Systems, ICUAS 2015, no. June 2015, pp. 1074–1083, 2015.

[5] S. P. Setyo Hariyadi, Sutardi, W. A. Widodo, and M. A. Mustaghfirin, “Aerodynamics analysis of the wingtip fence effect on UAV wing,” International Review of Mechanical Engineering, vol. 12, no. 10, 2018.

[6] S. P. Setyo Hariyadi, Sutardi, and W. A. Widodo, “Numerical study of flow characteristics around wing airfoil Eppler 562 with variations of rearward wingtip fence,” in AIP Conference Proceedings, vol. 1983, 2018.

[7] S. S. P. Hariyadi, Sutardi, and W. A. Widodo, “Drag reduction analysis of wing airfoil E562 with forward wingtip fence at cant angle variations of 75°and 90°,” in AIP Conference Proceedings, vol. 2001, 2018.

[8] G. K. Ananda, P. P. Sukumar, and M. S. Selig, “Measured aerodynamic characteristics of wings at low Reynolds numbers,” Aerospace Science and Technology, vol. 42, pp. 392–406, 2015.

[9] A. Choudhry, R. Leknys, M. Arjomandi, and R. Kelso, “An insight into the dynamic stall lift characteristics,” Experimental Thermal and Fluid Science, vol. 58, pp. 188–208, 2014.

[10] R. R. Leknys, M. Arjomandi, R. M. Kelso, and C. Birzer, “Dynamic- and post-stall characteristics of pitching airfoils at extreme conditions,” Proceedings of the Institution of Mechanical Engineers, Part G: Journal of Aerospace Engineering, vol. 232, no. 6, pp. 1171–1185, 2018.

[11] K. L. Tomek, A. H. Ullah, C. Fabijanic, and J. Estevadeordal, “Experimental investigation of dynamic stall on pitching swept finiteaspect-ratio wings,” AIAA Scitech 2020 Forum, vol. 1 PartF, no. January, pp. 1–35, 2020.

[12] P. Wang and Z. Shi, “Study of deep-stall characteristics and longitudinal special phenomena of T-tail aircraft,” 2010 IEEE International Conference on Mechatronics and Automation, ICMA 2010, pp. 59–64, 2010.

[13] R. T. Taylor and E. J. Ray, “A Systematic Study of the Factors Contributing to Post-Stall Longitudinal Stability of T-Tail Transport Configurations,” in AIAA Aircraft Design and Technology Meeting, pp. 15–18, 1965.

[14] J. Winslow, H. Otsuka, B. Govindarajan, and I. Chopra, “Basic understanding of airfoil characteristics at low Reynolds numbers (104– 105),” Journal of Aircraft, vol. 55, no. 3, pp. 1050–1061, 2018.

DOI: https://doi.org/10.71225/jstn.v2i4.120

[15] Huang S, Hu Y, Wang Y. Research on aerodynamic performance of a novel dolphin head-shaped bionic airfoil. Energy 2021;214. https://doi.org/10.1016/j. energy.2020.118179.
[16] Zhao M, Cao H, Zhang M, Liao C, Zhou T. Optimal design of aeroacoustic airfoils with owl-inspired trailing-edge serrations. Bioinspir Biomim 2021;16:56004. https://doi.org/10.1088/1748-3190/ac03bd.
[17] Fan M, Dong X, Li Z, Sun Z, Feng L. Numerical and experimental study on flow separation control of airfoils with various leading-edge tubercles. Ocean Eng 2022;252:111046. https://doi.org/10.1016/j.oceaneng.2022.111046.
[18] T. Rimadhani Hermawati, S. Hariyadi Suranto, and N. Pambudiyatno, "3 Dimensional Aerodynamic Analysis of Additional Slat and Slot on Airfoil Naca 23018 Using Computational Fluid Dynamic Method", *JSTN*, vol. 2, no. 2, pp. 26–36, May 2025.
[19] Zhang Y, Chen H, Fu S, Dong W. Numerical study of an airfoil with riblets installed based on large eddy simulation. Aerosp Sci Technol 2018;78:661–70. https://doi.org/10.1016/j.ast.2018.05.013.
[20] Sanei M, Razaghi R. Numerical investigation of three turbulence simulation models for S809 wind turbine airfoil. Proc Inst Mech Eng Part A J Power Energy 2018;232:1037–48. https://doi.org/10.1177/0957650918767301.
[21] S. N. Trysnavirensa, S. H. S. Putro, and N. Pambudiyatno, "The Effect of Triangular Vortex Generator Straight Arrangements on the NACA 0012 Airfoil Using a Smoke Generator", *JSTN*, vol. 2, no. 1, pp. 38–52, Feb. 2025.
[22] Mansi A, Aydin D. The impact of trailing edge flap on the aerodynamic performance of small-scale horizontal axis wind turbine. Energy Convers Manag 2022;256:115396. https://doi.org/10.1016/j.enconman.2022.115396.
[23] Reddy SR, Dulikravich GS, Abdoli A, Multi-winglets SH. Multi-objective optimization of aerodynamic shapes. In: 53rd AIAA Aerosp Sci Meet; 2015. https://doi.org/10.2514/6.2015-1489.
[24] Anitha D, Shamili GK, Ravi Kumar P, Sabari VR. Air foil Shape Optimization Using Cfd and Parametrization Methods. Mater Today: Proc 2018;5:5364–73. https://doi.org/10.1016/j.matpr.2017.12.122.
[25] A. Faadihillah, S. Hariyadi Suranto Putro, and A. Wulansari, "Aerodynamic Performance Optimization on NACA 2412 Airfoil Flap With The Addition of Riblets", *JSTN*, vol. 2, no. 3, pp. 17–34, Aug. 2025.
[26] Li J, He S, Martins JRRA. Data-driven constraint approach to ensure low-speed performance in transonic aerodynamic shape optimization. Aerosp Sci Technol 2019;92:536–50. https://doi.org/10.1016/j.ast.2019.06.008.
[27] Li X, Zhang L, Song J, Bian F, Yang K. Airfoil design for large horizontal axis wind turbines in low wind speed regions. Renew Energy 2020;145:2345–57. https:// doi.org/10.1016/j.renene.2019.07.163.
[28] Wei X, Wang X, Chen S. Research on parameterization and optimization procedure of low-Reynolds-number airfoils based on genetic algorithm and Bezier curve. Adv Eng Softw 2020;149:102864. https://doi.org/10.1016/j. advengsoft.2020.102864.

DOI: https://doi.org/10.71225/jstn.v2i4.120